Nanoscale Advances

ROYAL SOCIETY OF CHEMISTRY

PAPER

View Article Online
View Journal | View Issue

Cite this: *Nanoscale Adv.*, 2023, **5**, 3368

Amine-assisted catechol-based nanocoating on ultrasmall iron oxide nanoparticles for high-resolution T_1 angiography†

Hyunhong Kim,[a] Sunyoung Woo,[a] Hoesu Jung,[b] Hyo-Suk Ahn,[cd] Ning Chen,[a] HyungJoon Cho*[e] and Jongnam Park *[ae]

Received 27th November 2022
Accepted 19th April 2023

DOI: 10.1039/d2na00861k

rsc.li/nanoscale-advances

Surface engineered iron oxide nanoparticles (IONPs) with catecholic ligands have been investigated as alternative T_1 contrast agents. However, complex oxidative chemistry of catechol during IONP ligand exchange causes surface etching, heterogeneous hydrodynamic size distribution, and low colloidal stability because of Fe^{3+} mediated ligand oxidation. Herein, we report highly stable and compact (~10 nm) Fe^{3+} rich ultrasmall IONPs functionalized with a multidentate catechol-based polyethylene glycol polymer ligand through amine-assisted catecholic nanocoating. The IONPs exhibit excellent stability over a broad range of pHs and low nonspecific binding *in vitro*. We also demonstrate that the resultant NPs have a long circulation time (~80 min), enabling high resolution T_1 magnetic resonance angiography *in vivo*. These results suggest that the amine assisted catechol-based nanocoating opens a new potential of metal oxide NPs to take a step forward in exquisite bio-application fields.

Introduction

Magnetic resonance imaging (MRI) is one of the attractive non-invasive diagnostics techniques for soft tissues.[1] Specifically, high-resolution MR angiography has great promise for the diagnosis of blood vessel malfunctions for cardiovascular, renal, and oncological diseases.[2–5] Exogenous blood pool contrast agents (CAs) including paramagnetic and magnetic materials have been widely used to selectively improve vascular contrast in various MRI scans.[6,7] Specifically, T_1-weighted MRI with T_1 CAs has various advantages for accurate diagnosis, because their bright signal can be distinctly distinguished among tissues and also the suppressed blooming effect of T_1 CAs in comparison with T_2 CAs produces clear images.[8,9]

Ultrasmall iron oxide nanoparticles (IONPs) smaller than 5 nm have been exploited for T_1-weighted MR angiography due to their high content of ferric (Fe^{3+}) ions which have 5 unpaired electrons and a low net magnetic moment.[10] Their good biocompatibility and longer circulation time compared to traditional gadolinium or manganese ion complexes also provide advantages for using IONPs as T_1 magnetic CAs. To use IONPs in bio-applications, surface engineering should be considered because the surface of NPs determines bio-distribution and their fate *in vivo*.[11,12] Ligand grafting to NPs with catechol-tethered molecules has been one of the established surface treatment methods for metal oxide NPs since the pioneering research by Bing Xu *et al.* because the catechol anchor group exhibits strong binding affinity to metal oxides even under harsh aqueous conditions.[13,14] Nevertheless, heterogeneous and large hydrodynamic diameters, low coating yield, and even degradation of IONPs during the catechol mediated ligand grafting process have been reported.[15–19] The tricky and inconsistent phenomenon is derived from a complex catechol oxidative reaction pathway on the surface of IONPs owing to a similar redox potential between catechol and Fe^{3+}(ref. 20 and 21). Although newly designed catechol based surface ligands including cyclic brushes,[22] long polyethylene glycol (PEG) with a chain length above 2 kDa (ref. 23), and nitro-catechol derivatives[24] have been developed, catechol-based nanocoating on highly oxidative IONPs such as ultra-small IONPs or maghemite (γ-Fe_2O_3) NPs is still hampered by the presence of the high amount of Fe^{3+} which facilitates oxidation of catechol.[25] Despite the limitation, many studies about T_1 CA based IONPs have been successfully reported by repetitive purification or using samples with a large hydrodynamic diameter. In this regard, a convenient and efficient strategy for

[a]*School of Energy and Chemical Engineering, Ulsan National Institute of Science and Technology, Unist-gil 50 (100 Banyeon-ri), Eonyang-eup, Uljugun, Ulsan Metropolitan City 689-798, Republic of Korea. E-mail: jnpark@unist.ac.kr*

[b]*Preclinical Research Center, Daegu-Gyeongbuk Medical Innovation Foundation (KMEDIhub), Daegu, South Korea*

[c]*Division of Cardiology, Department of Internal Medicine, The Catholic University of Korea, Uijeongbu St. Mary's Hospital, Uijeongbu, Korea*

[d]*Catholic Research Institute for Intractable Cardiovascular Disease (CRID), College of Medicine, The Catholic University of Korea, Seoul, Republic of Korea*

[e]*Department of Biomedical Engineering, Ulsan National Institute of Science and Technology, Unist-gil 50 (100 Banyeon-ri), Eonyang-eup, Uljugun, Ulsan Metropolitan City 689-798, Republic of Korea*

† Electronic supplementary information (ESI) available: Details of additional characterization. See DOI: https://doi.org/10.1039/d2na00861k

the gram-scale coating method on NPs is required for reproducibility of data and wide application of inorganic nanocrystals.

Recently, we reported that an amine-assisted catechol-based nanocoating (AACN) provides a molecularly smooth and robust coating layer on metal oxide substrates and nanoparticles.[26,27] In the AACN mechanism, the key roles of separated amine in AACN are enhancement of catechol adhesion, suppression of polymerization derived from catechol, and additional stabilization through an *in situ* generated catechol-amine adduct. Therefore, the detachment of catecholic ligands from NPs by iron ion catalyzed oxidation of catechol on the surface of Fe^{3+} rich iron oxides including 3 nm-sized IONPs can be overcome by the method during the coating process. Herein, we report ultrasmall IONPs coated with a multidentate catechol-based PEG brush polymer (MCP) *via* the AACN method. The surface engineered IONPs exhibited compact, monodisperse hydrodynamic diameters, and high colloidal stability in biological media. Notably, the method was demonstrated by yielding more than 1 g of surface engineered IONPs per one-batch reaction due to the support of nucleophilic amine. After low nonspecific binding and non-toxicity of the IONPs were confirmed, the obtained IONPs were used as a T_1 MRI CA for *in vivo* high-resolution angiography.

Experimental section/methods

Materials

Poly(ethylene glycol) methyl ether acrylate (average $M_n = 480$) (APEG) and 2-(2-aminoethoxy) ethanol (AEE) were purchased from Sigma-Aldrich. Dopamine methacrylamide (DMA) and dibenzyl trithiocarbonate (DTC) were synthesized, as previously reported.[28,29] Organic solvents were obtained from SAMCHUN CHEMICALS. Azobisisobutyronitrile (AIBN) was obtained from Junsei. PEG (2 kDa)-derivatized phosphine oxide (PO-PEG) was synthesized following the literature.[30]

Synthesis of a multidentate catechol-based PEG brush polymer

DMA (0.6 mmol), APEG (2.4 mmol), DTC (0.15 mmol), and AIBN (0.075 mmol) were mixed in a 10 ml vial and then dissolved in 2 ml of dimethylformamide (DMF). The resulting mixture was transferred to an ampule; the ampule was subjected to 3 cycles of freeze–pump–thaw, followed by sealing with a gas torch under vacuum, and then reacting in an oil bath at 70 °C for 12 h. After the reaction, the crude solution was precipitated with diethyl ether and washed three times.

Synthesis of ultrasmall iron oxide nanoparticles

3 nm-sized IONPs were synthesized using a protocol previously reported in the literature.[10] Iron oleate (1 mmol) and oleyl alcohol (6 mmol) were dissolved in 5 g of diphenyl ether. The mixture was heated to 250 °C at a heating rate of 3.3 °C min^{-1} under an Ar atmosphere and kept at that temperature for 30 min. The resulting solution was cooled under inert conditions, and the product was collected by centrifugation in acetone and ethanol for 3 min at 5000 rpm.

Synthesis of 12 nm-sized iron oxide nanoparticles

The 12 nm-sized IONPs were synthesized using a thermal decomposition method in the literature with a slight modification.[31] Iron oleate (1 mmol) and oleic acid (1 mmol) were dissolved in 5 g of 1-octadecene. The mixture was heated to 320 °C at a heating rate of 3.3 °C min^{-1} in an inert atmosphere and kept for 30 min at 320 °C. The resulting solution was cooled under argon atmosphere conditions. The final product was collected by centrifugation using an acetone solvent.

Surface engineering of IONPs with a multidentate catechol-based PEG brush polymer

Oleic-acid-capped IONPs (3 mg) in 300 μl of chloroform were mixed with 0.002 mmol of multidentate catechol-based PEG brush polymer (MCP) and 0.2 mmol of AEE. The solution was allowed to react overnight in a glass vial at 60 °C with magnetic stirring. The crude solution was precipitated with ethyl ether to remove chloroform, and the pellet was dispersed in deionized water (D.W.). The aqueous solution was purified using a centrifugal membrane filter (Amicon Ultra-4 50k) at 4000 rcf.

Instrumentation and analyses

The sizes of NPs were measured by transmission electron microscopy (TEM, JEOL, JEM-2100) conducted at 200 kV, for which the dispersed samples were placed on a carbon copper grid for measurement. The hydrodynamic diameter and zeta-potential were studied using a Malvern Instruments Zetasizer Nano-ZS90 at 25 °C. XPS spectra were recorded on an ESCALAB 250XI (Thermo Fisher Scientific). Al Kα radiation (1486.6 eV) under ultrahigh vacuum (1.0×10^{-10} torr) was used, and spectra were measured in high-resolution mode (0.45 eV). FT-IR spectra were measured on a Varian 670/620 at room temperature. The molecular weight of the resultant polymers was measured using a GPC (Agilent 1200S system) at 25 °C. All samples before measurement were filtered using a 0.2 μm PTFE syringe filter. Tetrahydrofuran was used as an eluent, and polystyrene standards were used for calibration. The high power X-ray diffraction (HPXRD) data were recorded with a Rigaku D/MAX 2500 V/PC using Cu Kα radiation ($\lambda = 1.54180$ Å). X-ray Photoelectron Spectroscopy (XPS) spectra were obtained on an ESCALAB 250XI (Thermo Fisher Scientific). Al Kα radiation (1486.6 eV) under ultrahigh vacuum (1.0×10^{-10} torr) was used, and spectra were measured in a high-resolution mode (0.45 eV). Thermogravimetric analysis (TGA) measurements were conducted using a TA instruments Q500 analyzer. Freeze-dried samples were placed into an alumina pan and heated from 35 to 700 °C at a heating rate of 10 °C min^{-1} under a nitrogen atmosphere.

Serum binding test

MCP-coated 3 nm IONPs (20 mM Fe) were incubated in 100% FBS at 37 °C for 30 min. Fast protein liquid chromatography

(FPLC) with a Superose 6 10/300 GL column was performed for analysis, and 1× PBS was used as an eluent. All of the samples were filtered through 0.2 μm cellulose acetate syringe-filters before injection into the FPLC.

Colloidal stability test with FPLC

3 nm IONP@MCP/AEE and 3 nm IONP@PO-PEG were injected into the FPLC with a Sephadex G-25 column. Eluent of the system is 1× PBS. All of the samples were filtered through 0.2 μm cellulose acetate syringe-filters before injection into the FPLC.

Cytotoxicity test

100 μl of a HeLa cell suspension was dispensed in a culture well (5×10^3 cells per well). After 1 day settling, the HeLa cells were incubated with IONPs or 1 μM of doxorubicin at 37 °C and 5% CO_2 in an incubator. After 24, 48, and 72 h of incubation, 2 μl of CCK-8 solution was added to each well of the plate. The plate was incubated in an incubator for 4 h. Then, absorbance at 450 nm was recorded using a multiplate reader (Tecan, Infinite M200).

MR relaxivity

The relaxivity values of 3 nm-sized IONP@MCP/AEE were measured using a 3 T MRI scanner (Philips' Achieva, 3 T). The *in vitro* phantom image was obtained for the IONPs to calculate the r_1 and r_2 of the IONPs for *in vivo* MR imaging. For the IONPs, 0.1125, 0.225, 0.45, and 0.9 mM Fe were prepared. A volume coil recorded the T_1-weighted MR images of the phantom with the 3 T MRI scanner using the Turbo inversion recovery (TIR) sequence. The imaging parameters were as follows: $T_I = 50$, 100, 150, 200, 300, 400, 500, 650, 800, 1000, 1200, 1400, 1600, 1800, 2000, 2200, 2400 and 2600 ms, echo time (T_E) = 10 ms, flip angle = 90°, repetition time (T_R) = 3000 ms. The T_2-weighted and T_2^*-weighted MR images of the phantom were prepared in water. The r_2 and r_2^* relaxivity values were obtained using a 3 T MRI scanner with a volume coil. Multi-echo-spin-echo (MESE) and multi-echo gradient echo (MEGE) sequences were used to measure T_2 and T_2^*. The measurement parameters of T_2 were as follows: T_E = 17.56, 23.41, 29.26, 35.11, 40.96, 52.67, 58.52, 64.37, and 70.22 ms, flip angle = 90°, T_R = 3388 ms. The measurement parameters of T_2^* were as follows: T_E = 5.24, 10.19, 15.14, 20.09, 25.04, 30, 34.95, 33.9, 44.85, and 49.8 ms, flip angle = 60°, T_R = 3000 ms.

In Vivo MR imaging

T_1-weighted fast-field echo (T1W-FFE) images of male Sprague-Dawley rats and mice (Orient Bio, Inc., Seongnam, South Korea) weighing 140–300 g were acquired using a volume coil on the 3 T MRI scanner before and after the injection of the IONPs. The Institutional Animal Care and Use Committee of the Ulsan National Institute of Science & Technology approved the *in vivo* animal experiments conducted in this study (UNISTIACUC-21-04). The IONP@MCP/AEE (22.4 Fe mM, dose = 2.5 mg Fe per kg) was injected into a peripheral vein at a dose of 2× rat body weight (μL). The T1W-FFE images were obtained at an interval of 8 min after the injection of IONPs to validate the clearance of the IONPs from the vascular system. The images were reconstructed using a maximum intensity projection (MIP) protocol with MATLAB (R2012a). The imaging parameters of T1W-FFE were as follows: flip angle = 25, T_R = 25 ms, T_E = 3.6 ms, field of view (FOV) = 150 × 150 × 35 mm^3, matrix = 640 × 640 × 35, and number of excitations (NEX) = 1.

Results and discussion

The reversible addition–fragmentation chain-transfer (RAFT) polymerization method was chosen (Scheme 1(a)) for the preparation of MCP.[32] RAFT polymerization is attractive owing to its functional versatility due to the existence of a vast library of vinyl monomers and narrow size distribution. MCP with a molecular weight of 8620 and a polydispersity index (M_w/M_n) of 1.27 was synthesized through our previous work; the polymer consists of a 20% mole fraction of the catechol function and an 80% mole fraction of the PEG monomer.[32,33] IONPs were prepared using a modified thermal decomposition of iron oleate with oleyl alcohol.[10] Fig. S1a in the ESI† shows the typical transmission electron microscopy (TEM) image of the resultant as-syn IONPs with an average diameter of 3.2 + 0.47 nm. Ligand exchange with the uniform synthetic ligand and monodisperse IONPs give a synergistic effect for exquisite control of the surface properties of NPs using the AACN method.

The representative mechanism of AACN on IONPs using MCP and amine additives (AA); 2-(2-aminoethoxy) ethanol (AEE) is illustrated in Scheme 1(b). The main concept of AACN is the amine-mediated redox modulation of catechol during the surface engineering process, leading to suppressed cohesion and enhanced adhesion.[26] In Scheme 1(c), a detailed mechanistic description of the catecholic nanocoating with and without AA is shown. First, the coordination bond between catechol and the iron ion is facilitated because the basicity of AA promotes deprotonation of hydroxyl groups of catechol.[34] Then, coordinated catechol is oxidized to the semiquinone form due to a similar redox potential between catechol and Fe^{3+} (~0.75 V).[20] In the presence of AA, the semi-quinones react with the nucleophilic AA and the oxidized catechol is recovered through the formation of the catechol-amine adduct. The generated adduct further stabilizes the coordination bond through its electron donating effects of the amine substituent to iron ions[26] because the partially reduced ferric ion can resist acquiring an electron from the catechol.[35] In contrast, consecutive electron transfers occur between semi-quinone and the iron ions in the absence of AA and the resultant quinones are detached from the IONPs due to a loss of affinity. Oxidative intra- and intermolecular polymerization processes were also potential reaction pathways from the resultant quinones and significant NP agglomeration occurs.

Surface engineering of 3 nm-sized oleic acid-capped IONPs with MCP in the presence of AA is shown in Fig. 1. As-syn IONPs dispersed in the hexane phase perfectly transferred to the water phase after ligand exchange reaction with MCP and AEE. No sign of aggregation was observed in IONP@MCP/AEE however,

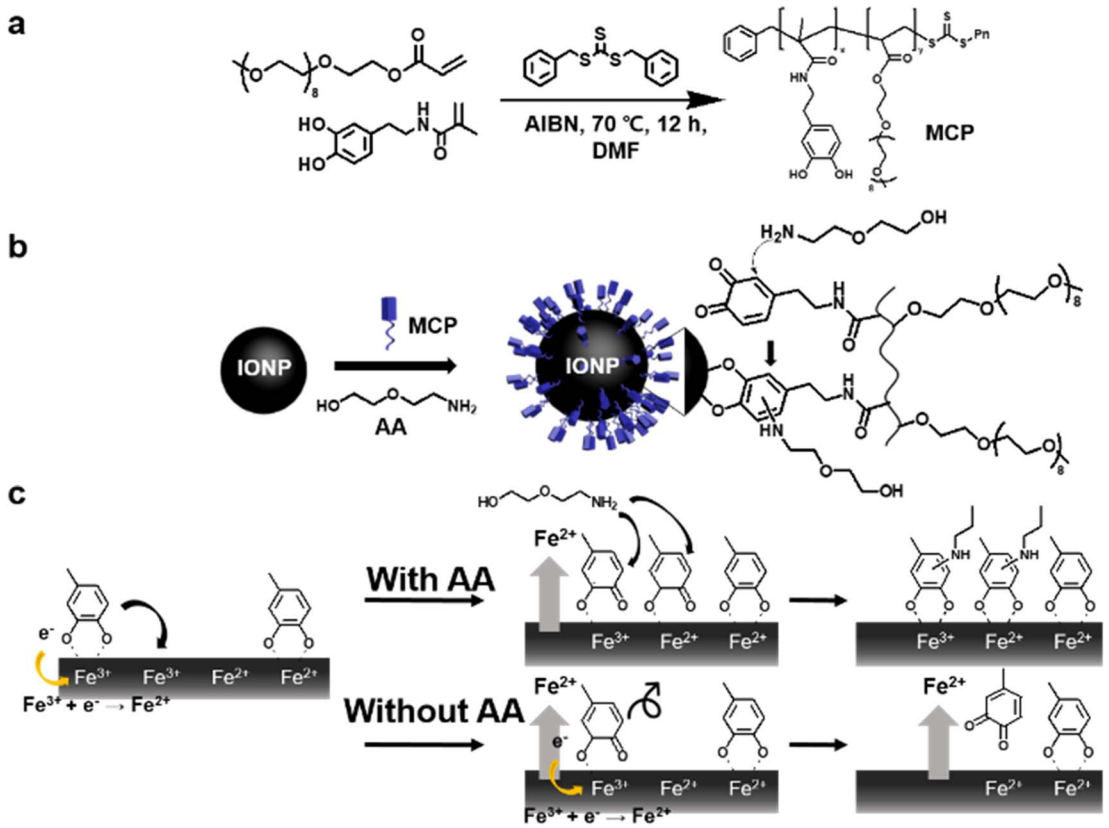

Scheme 1 (a) Synthesis of MCP by RAFT polymerization, (b) schematic illustration of the AACN procedure with MCP and AEE on IONPs, and (c) a detailed mechanistic description of catecholic nanocoating with and without AA.

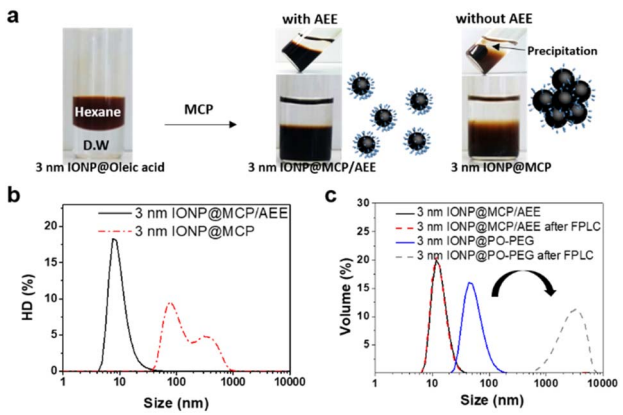

Fig. 1 (a) Photograph of 3 nm sized-IONPs dispersed in hexane (left). Photograph of 3 nm sized-IONPs after MCP coating with AEE (middle) and without AEE (right). (b) DLS data of IONP@MCP/AEE and IONP@MCP. (c) DLS data after colloidal stability evaluation *via* FPLC.

a significant precipitation occurred in the case of the MCP coating without AA (Fig. 1(a)). Dynamic light scattering (DLS) measurements show that the IONP@MCP/AEE has a monomodal and narrow size distribution in D. W. with a hydrodynamic diameter (HD) of 10.1 nm (Fig. 1(b)). The compact HD has the optimal size for a long blood half-life of CAs because NPs with HD larger than 100 nm are rapidly cleared *via* mononuclear phagocytic systems including Kupffer cells in liver, spleen, and bone marrow.[36] In addition, the HD of NPs less than 6 nm is inadequate for long circulation because they are generally eliminated through urinary excretion.[37] On the other hand, DLS of IONP@MCP shows a heterogeneous size distribution and signs of severe agglomeration; 98.4 nm, 63%, and 370 nm, 37% (Fig. 1b). The surface charge of the polymer-coated ultrasmall IONPs was measured using the zeta-potential. The surface charge of the NPs is −0.74 mV which is slightly negative to neutral. The neutral PEG surface is advantageous for *in vivo* application due to its non-specific binding properties. TEM data for IONP@MCP/AEE shows an average particle size of 3.4 + 0.40 nm (Fig. S1b in the ESI†). The morphology of the IONPs is maintained and there was no evidence of etching after ligand exchange from the TEM image. From the above data, we concluded that the AACN with the MCP could be applied on ultrasmall IONPs. FT-IR analysis was conducted on IONP@Oleic acid, MCP, and IONP@MCP/AEE to explore the molecular structure of the surface coating layer (Fig. S2a in the ESI†). The highlighted region in red indicates the optimal window for analyzing the aromatic groups in catechol (Fig. S2a and b in the ESI†). The vibration at 850 cm^{-1} for the MCP reduced after AACN on IONPs and it indicates that a substituent change in the aromatic group occurred when AEE was used

during the MCP coating process.[38] The vibration band at 800 cm^{-1} is from the Fe–OH bond in the IONPs.[39]

TGA, XPS and XRD were used to elucidate the structural information of IONP@MCP/AEE. TGA was performed on lyophilized surface modified IONPs to determine the organic contents. The weight loss at 200–700 °C of 3 nm sized IONP@MCP/AEE was about 70% (Fig. S3 in the ESI†). The trend of the weight loss curve is similar to TGA data of PEGylated 3 nm sized NPs reported previously.[19] XPS analysis was used to characterize the chemical environments of the coating layer of the IONPs (Fig. S4 in the ESI†). The N 1s XPS spectra of the IONP@MCP/AEE were deconvoluted into peaks at 399.2 and 400.0 eV, which indicate C–N and HN–C=O, respectively (Fig. S4a in the ESI†). A newly developed 400.0 eV photopeak compared to MCP indicates that a secondary amine was made *in situ* during the coating process because the signal at 399.2 eV is attributed to the amide group of MCP (Fig. S4b in the ESI†).[26] In the Fe 2p state in XPS spectra, there are five peaks at 709.9, 711.5, 718.2, 724, and 733.9 eV. The existence of a satellite peak near 718 eV is evidence of maghemite (Fig. S4c in the ESI†).[40] Additionally, the Fe $2p_{1/2}$ state from 724 eV to 733.9 eV confirms the presence of iron oxide.[40] XRD patterns of 3 nm IONP@MCP/AEE and 3 nm IONP@oleic acid are shown in Fig. S5 in the ESI.† The XRD pattern of 3 nm-sized IONP@oleic acid demonstrated the maghemite (γ-Fe_2O_3; JCPDS no. 39-1346) crystal structure.[10] As expected, the surface modified IONP shows broad and low intensity due to the high mass of the PEG.[41]

To further investigate the relative colloidal stability of IONP@MCP/AEE, we prepared PEG (2 kDa)-derivatized phosphine oxide (PO-PEG) stabilized 3 nm IONPs.[30] Each sample was injected into a fast protein liquid chromatograph (FPLC) with a Sephadex G-25 column and the collected samples after passing through the column with 1× PBS eluent were analysed by DLS. The dextran resin column (Sephadex G-25) has high affinity to metal oxide, so it is possible to replace the original surface ligands on NPs with hydroxyl groups of dextran.

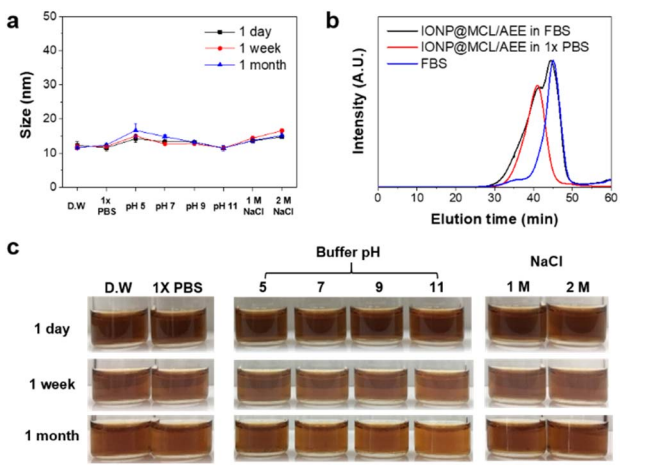

Fig. 2 (a) HD of IONP@MCP/AEE at various pHs and salt concentrations over time. (b) Serum binding test through size exclusion chromatography. (c) Stability evaluation of IONP@MCP/AEE at various pHs and salt concentrations.

Therefore, the method can be used to evaluate the colloidal stability of NPs.[42] Interestingly, IONP@MCP/AEE maintained its HD value after passing through the FPLC column however, IONP@PO-PEG lost its colloidal stability after passing through the column (Fig. 1(c)). Colloidal stability and nonspecific affinity of the IONPs were evaluated before using the IONPs in *in vivo* applications (Fig. 2). The IONP@MCP/AEE was stable over a wide pH range (5–11) and at NaCl concentrations up to 2 M for at least one month (Fig. 2(a) and (c)). Colloidal stability of MCP nanocoated 8.5 nm and 12 nm-sized IONPs with AEE was also tested and showed similar stability to that of 3 nm IONP@MCP@AEE (Fig. S6 in the ESI†). Next, we substantiated the possibility of a large-scale ligand exchange process through scaling up the batch reaction for IONP@MCP/AEE by a factor of 200 (Fig. S7 in the ESI†). We successfully obtained 1 gram of product and confirmed that the product is comparable to the HD from the small-scale ligand exchange.

A serum binding test for nanocoated IONPs can determine their low nonspecific affinity in protein including in solutions such as fetal bovine serum (FBS) which is a widely used serum for cell experiments.[43] Size exclusion chromatography was used to investigate protein adsorption on NPs by comparing the change in size.[44] The IONP@MCP/AEE in 1× PBS and IONP@MCP/AEE in FBS solution were incubated at 37 °C for 30 min and then analyzed with FPLC (Fig. 2(b)). Interestingly, both IONPs in 1x PBS and FBS showed almost the same elution time (41 min) and a monodisperse size distribution, meaning IONP@MCP/AEE has corona-free characteristics. Unstable or non-passivated NPs can interact with various proteins and lipids present in serum *in vivo*, resulting in large corona structures.[45] The corona causes loss of targeting ability and also accumulation of NPs, so the resultants are easily recognized by the mononuclear phagocytic system and finally removed.[46,47] Unpredictable localization and reduced circulation time of NPs *in vivo* also adversely affected the MR imaging process. The completely suppressed nonspecific interaction of NPs with proteins comes from the dense amine-assisted MCP coating layer, which contains PEG molecules of a relatively short chain length ($n \sim 9$) compared to commonly available long PEG molecules ($n > 50$). The MCP, brush copolymer ligands with short chain length behave like hard spheres because dense PEG brush chains have a stretched chain conformation on NPs.[48] It was proved that the MCP exhibits autophobic dewetting properties under P/N $\gg 1$, so macromolecules like proteins can be repelled from the IONP@MCP/AEE.[49]

In vitro cell viability and cytotoxicity tests were performed using HeLa cells to prove the non-toxicity of IONP@MCP/AEE before *in vivo* imaging. The biocompatibility of MCP coated

Table 1 MR relaxation of IONP@MCP/AEE at 1.4 T with various sized MCP coated IONPs with AEE

Size (nm)	r_1 (mM^{-1} s^{-1})	r_2 (mM^{-1} s^{-1})	r_2/r_1
3	3.42	13.7	4.02
8.5	16.7	64.1	3.84
12	11.8	123	10.4

Table 2 MR phantom test of 3 and 12 nm sized IONP@MCP/AEE and DOTAREM on a 3.0 T clinical MRI scanner

	r_1 (mM^{-1} s^{-1})	r_2 (mM^{-1} s^{-1})	r_2/r_1
3 nm IONP	2.34	26.1	8.53
12 IONP	2.54	142	55.8
DOTAREM	3.78	4.43	1.17
SPION (5–10 nm)	6.84	39.68	5.8

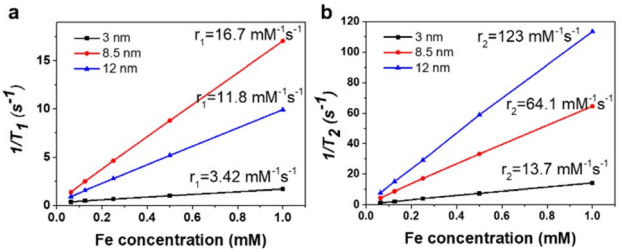

Fig. 3 (a) Plots of r_1 values and (b) r_2 values of MCP nanocoated IONPs with AEE.

IONPs *via* the AACN method has been confirmed in our previous literature through the MTT assay using three human cell lines (A549, Huh-7, and SH-SY5Y), and also hematological analysis and histopathological observation.[50] In this paper, *in vitro* cell viability and cytotoxicity tests were performed using HeLa cells following other studies to check the non-toxicity of ultrasmall IONP@MCP/AEE before *in vivo* imaging.[19,51,52] The CCK-8 assay with HeLa cells showed that the IONPs are biocompatible for up to 3 days even at 100 μg Fe per ml (Fig. S8 in the ESI†). We then studied the contrast ability of the IONPs by measurement of relaxivity. The relaxation time was recorded on a 1.4 T magnet NMR minispec and 3.0 T MR scanner (Tables 1 and 2). Fig. 3 and Table 1 summarize the relaxometric properties of 3, 8, and 12 nm sized IONP@MCP/AEE on a 1.4 T minispec. The r_1 value for 3 nm-sized IONPs was 3.42 mM^{-1} s^{-1} comparable to that of the 3 nm-sized IONPs reported in other papers.[10,45] A low r_2/r_1 value is necessary for a satisfactory T_1-weighted MR image, and the r_2 value for 3 nm-sized IONPs showed a lower value than those for the 8.5 nm and 12 nm sized IONPs as expected. The *in vitro* phantom test of IONP, SPION and DOTAREM was performed to calculate the r_1 and r_2 of the IONPs for *in vivo* MR imaging and a significant enhancement of T_1 contrast was observed in 3 nm IONPs and DOTAREM (Gd-DOTA) (Table 2). Dextran coated SPION was synthesized by a co-precipitation method to confirm the effect of surface modification.[1] As shown in Table 2, the r_2/r_1 of SPION at 3 T is 5.8 and this value is higher than the r_2/r_1 of 3 nm and 8.5 nm sized IONPs. From the result, 3 nm IONP@MCP/AEE can be used as an efficient T_1 CA than the others.

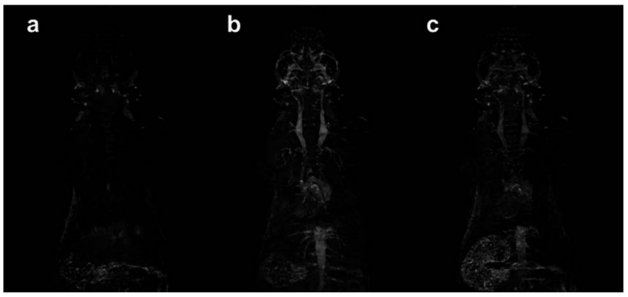

Fig. 4 2D-MIP *in vivo* angiography (a) before, (b) after–before injection of ultrasmall IONP@MCP/AEE, and (c) 1 hour after–before injection of the NPs. 2.5 mg Fe per kg of sample is injected into rats.

The blood pool T_1 MR image was recorded using a 3 T MRI instrument by intravenous injection of the IONPs (2.5 mg Fe per kg) into a rat through the tail. Highly positive enhanced contrast in whole blood vessels was obtained as soon as the IONPs were injected (Fig. 4(a) and (b)). The bright contrast-enhanced MR signal intensity over the blood vessel was maintained at a high value for more than 1 hour as shown in Fig. 4(c). According to the data, the nanocoated 3 nm sized IONPs showed their potential as an efficient *in vivo* T_1 CA. The blood vessel imaging can provide important information related to diseases such as renal failure, tumors angiogenesis, and myocardial infarction.[4,5,41] However, conventional imaging agents, like

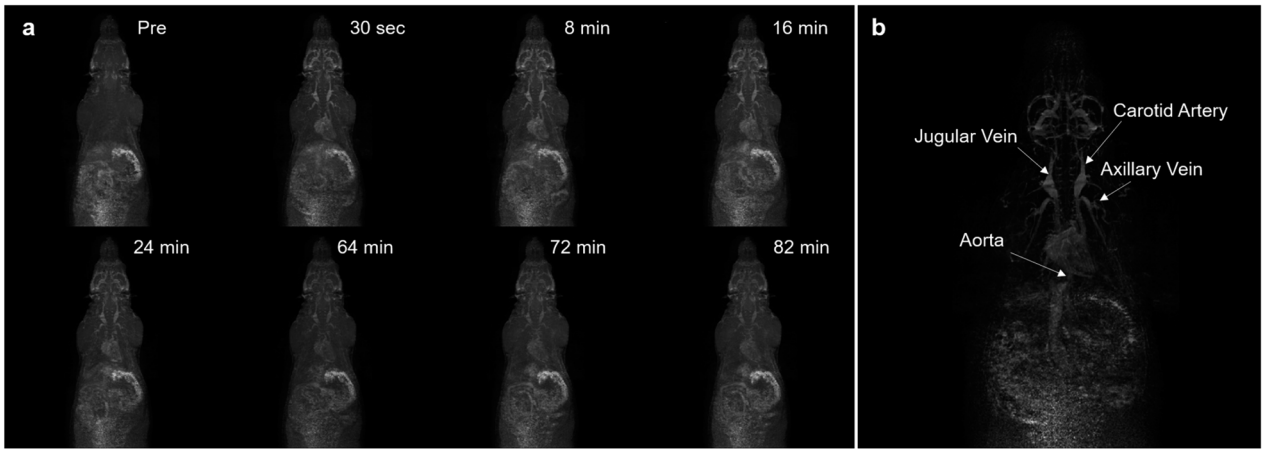

Fig. 5 (a) IONP enhanced 2D-MIP angiography with a dynamic time-resolved MR sequence. (b) 2D-MIP angiography of post–pre MR *in vivo* images through 3 nm-sized MCP/AEE coated IONPs after injection. 2.5 mg Fe per kg of sample is injected into rats.

DOTAREM, have limitations in terms of toxicity and a short acquisition window to obtain a high-resolution MR angiogram because Gd-DOTA is rapidly excreted as urine.[53] The control experiments by DORAREM are demonstrated in Fig. S9 in the ESI.† The pre image in Fig. S9 in the ESI† is before DOTAREM injection and post image (30 s) is after DOTAREM injection. The doses injected into the peripheral vein of an SD rat were 100 μmol kg^{-1} for Gd-DOTA. In the case of DOTAREM, the resultant vessel/tissue contrast was negligible because of the fast washout of the agent in rodents. In Fig. 5(a), a dynamic time-resolved MR sequence was used to track IONP-enhanced MR images up to 82 min after injection of IONPs. The MR enhancement signal of the vessel area was maintained over 80 min, indicating that the IONP@MCP/AEE is beneficial for achieving steady-state imaging due to the improved circulation time of IONPs (Fig. S10a and b in the ESI†), and the HD with 10.1 nm keeps excretion of NPs through the kidneys and perfusion into the tissue to a minimum.[36,53,54] As a result, the aorta, axillary vein, jugular vein, carotid artery, and cerebral veins were clearly detected in a two-dimensional (2D) maximum intensity projection (MIP) image (Fig. 5(b)). Although, SPION also has a long circulation time (Fig. S11 in the ESI†), the AANC surface modification method can be applied to highly uniform and various nanocrystals synthesized in high-boiling point organic solvents for bio and electronic applications.[27]

Conclusion

In summary, MCP-coated IONPs using the AACN method were investigated and their potential as a high resolution T_1 CA *in vivo* was demonstrated. Separated amine additives and catecholic ligands successfully developed a compact and molecularly smooth coating layer on highly oxidative ultrasmall IONPs by modulation of catechol redox chemistry. The resulting product exhibited high colloidal stability under physiological conditions and ultralow non-specific binding properties due to the short brush PEG chain of MCP. We further demonstrated the *in vivo* application potential through MR angiography using the surface engineered IONPs. The long circulation time over 80 min and highly enhanced resolution of vascular details can hold great promise in the clinical MRI field. We anticipate that the surface engineering method *via* catechol derivatives can extend the application of IONPs to various fields.

Author contributions

The manuscript was written through contributions of all authors. All authors have given approval to the final version of the manuscript.

Conflicts of interest

There are no conflicts to declare.

Acknowledgements

This work was supported by the Korea Medical Device Development Fund grant funded by the Korea government (the Ministry of Science and ICT, the Ministry of Trade, Industry and Energy, the Ministry of Health & Welfare, the Ministry of Food and Drug Safety) (Project Number: 1711139068, KMDF_PR_20210525_0001). This work was also supported by the National Research Foundation (NRF) grants funded by the Korean government [No. NRF-2017M3A7B6052456].

References

1 H. Jung, B. Park, C. Lee, J. Cho, J. Suh, J. Park, Y. Kim, J. Kim, G. Cho and H. Cho, *Nanomedicine*, 2014, **10**, 1679–1689.
2 J. P. Laissy, J. M. Idée, A. Loshkajian, S. Benderbous, S. Chillon, H. Beaufils and E. Schouman-Claeys, *J. Magn. Reson. Imaging*, 2000, **12**, 278–288.
3 E.-J. Cho, J. Yang, K. A. Mohamedali, E.-K. Lim, E.-J. Kim, C. J. Farhangfar, J.-S. Suh, S. Haam, M. G. Rosenblum and Y.-M. Huh, *Invest. Radiol.*, 2011, **46**, 441–449.
4 C. Zhang, M. Jugold, E. C. Woenne, T. Lammers, B. Morgenstern, M. M. Mueller, H. Zentgraf, M. Bock, M. Eisenhut, W. Semmler and F. Kiessling, *Cancer Res.*, 2007, **67**, 1555–1562.
5 J. D. Turner, W. J. Rogers, J. A. Mantle, C. E. Rackley and R. O. Russell Jr, *Chest*, 1980, **77**, 58–64.
6 J. Y. Park, M. J. Baek, E. S. Choi, S. Woo, J. H. Kim, T. J. Kim, J. C. Jung, K. S. Chae, Y. Chang and G. H. Lee, *ACS Nano*, 2009, **3**, 3663–3669.
7 Y. Song, Y. J. Kang, H. Jung, H. Kim, S. Kang and H. Cho, *Sci. Rep.*, 2015, **5**, 15656.
8 C. H. Cunningham, T. Arai, P. C. Yang, M. V. McConnell, J. M. Pauly and S. M. Conolly, *Magn. Reson. Med.*, 2005, **53**, 999–1005.
9 N. Lee, H. Kim, S. H. Choi, M. Park, D. Kim, H.-C. Kim, Y. Choi, S. Lin, B. H. Kim, H. S. Jung, H. Kim, K. S. Park, W. K. Moon and T. Hyeon, *Proc. Natl. Acad. Sci.*, 2011, **108**, 2662–2667.
10 B. H. Kim, N. Lee, H. Kim, K. An, Y. I. Park, Y. Choi, K. Shin, Y. Lee, S. G. Kwon, H. B. Na, J.-G. Park, T.-Y. Ahn, Y.-W. Kim, W. K. Moon, S. H. Choi and T. Hyeon, *J. Am. Chem. Soc.*, 2011, **133**, 12624–12631.
11 M. A. Boles, D. Ling, T. Hyeon and D. V. Talapin, *Nat. Mat.*, 2016, **15**, 141–153.
12 S. Laurent, D. Forge, M. Port, A. Roch, C. Robic, L. Vander Elst and R. N. Muller, *Chem. Rev.*, 2008, **108**, 2064–2110.
13 C. Xu, K. Xu, H. Gu, R. Zheng, H. Liu, X. Zhang, Z. Guo and B. Xu, *J. Am. Chem. Soc.*, 2004, **126**, 9938–9939.
14 J. Zhou, Z. Lin, Y. Ju, M. A. Rahim, J. J. Richardson and F. Caruso, *Acc. Chem. Res.*, 2020, **53**, 1269–1278.
15 M. D. Shultz, J. U. Reveles, S. N. Khanna and E. E. Carpenter, *J. Am. Chem. Soc.*, 2007, **129**, 2482–2487.
16 J. Xie, C. Xu, Z. Xu, Y. Hou, K. L. Young, S. X. Wang, N. Pourmand and S. Sun, *Chem. Mater.*, 2006, **18**, 5401–5403.
17 A. K. L. Yuen, G. A. Hutton, A. F. Masters and T. Maschmeyer, *Dalton Trans.*, 2012, **41**, 2545–2559.

18 M. Sara, D. Carmelo, M. F. Anna, P. Alessandra and P. Alessandro, *Nanotechnology*, 2013, **24**, 105702.
19 P. Li, P. Chevallier, P. Ramrup, D. Biswas, D. Vuckovich, M.-A. Fortin and J. K. Oh, *Chem. Mater.*, 2015, **27**, 7100–7109.
20 H. Powell and M. Taylor, *Aust. J. Chem.*, 1982, **35**, 739–756.
21 J. Yang, M. A. Cohen Stuart and M. Kamperman, *Chem. Soc. Rev.*, 2014, **43**, 8271–8298.
22 G. Morgese, B. Shirmardi Shaghasemi, V. Causin, M. Zenobi-Wong, S. N. Ramakrishna, E. Reimhult and E. M. Benetti, *Angew. Chem., Int. Ed.*, 2017, **56**, 4507–4511.
23 N. Gal, A. Lassenberger, L. Herrero-Nogareda, A. Scheberl, V. Charwat, C. Kasper and E. Reimhult, *ACS Biomater. Sci. Eng.*, 2017, **3**, 249–259.
24 E. Amstad, T. Gillich, I. Bilecka, M. Textor and E. Reimhult, *Nano Lett.*, 2009, **9**, 4042–4048.
25 E. Amstad, A. U. Gehring, H. Fischer, V. V. Nagaiyanallur, G. Hähner, M. Textor and E. Reimhult, *J. Phys. Chem. C*, 2010, **115**, 683–691.
26 H. Kim, H. Kim, S. H. Kim, J. M. Park, Y. J. Jung, S. K. Kwak and J. Park, *Chem. Mater.*, 2021, **33**, 952–965.
27 H. Kim, S. H. Yook, H. Y. Kim, Y. Choi, Y. Lim, Y. Hwang, J. Kim, K. Y. Lee, S. S. Jang, J. Park and J. Y. Kim, *Adv. Electron. Mater.*, 2022, **8**, 2200171.
28 N. Aoyagi and T. Endo, *J. Polym. Sci., Part A: Polym. Chem.*, 2009, **47**, 3702–3709.
29 H. Lee, B. P. Lee and P. B. Messersmith, *Nature*, 2007, **448**, 338–341.
30 H. B. Na, I. S. Lee, H. Seo, Y. I. Park, J. H. Lee, S.-W. Kim and T. Hyeon, *Chem. Commun.*, 2007, 5167–5169.
31 J. Park, K. An, Y. Hwang, J.-G. Park, H.-J. Noh, J.-Y. Kim, J.-H. Park, N.-M. Hwang and T. Hyeon, *Nat. Mater.*, 2004, **3**, 891–895.
32 N. K. Kwon, H. Kim, I. K. Han, T. J. Shin, H.-W. Lee, J. Park and S. Y. Kim, *ACS Macro Lett.*, 2018, **7**, 962–967.
33 H.-K. Na, H. Kim, J. G. Son, J. H. Lee, J.-K. Kim, J. Park and T. G. Lee, *Appl. Surf. Sci.*, 2019, **483**, 1069–1080.
34 J. Yu, W. Wei, M. S. Menyo, A. Masic, J. H. Waite and J. N. Israelachvili, *Biomacromolecules*, 2013, **14**, 1072–1077.
35 J. Fouineau, K. Brymora, L. Ourry, F. Mammeri, N. Yaacoub, F. Calvayrac, S. Ammar-Merah and J. M. Greneche, *J. Phys. Chem. C*, 2013, **117**, 14295–14302.
36 K. P. García, K. Zarschler, L. Barbaro, J. A. Barreto, W. O'Malley, L. Spiccia, H. Stephan and B. Graham, *Small*, 2014, **10**, 2516–2529.
37 M. Longmire, P. L. Choyke and H. Kobayashi, *Nanomedicine*, 2008, **3**, 703–717.
38 Q. Wei, K. Achazi, H. Liebe, A. Schulz, P.-L. M. Noeske, I. Grunwald and R. Haag, *Angew. Chem., Int. Ed.*, 2014, **53**, 11650–11655.
39 X. Huang, A. Schmucker, J. Dyke, S. M. Hall, J. Retrum, B. Stein, N. Remmes, D. V. Baxter, B. Dragnea and L. M. Bronstein, *J. Mater. Chem.*, 2009, **19**, 4231–4239.
40 S. Chandrasekaran, S. H. Hur, E. J. Kim, B. Rajagopalan, K. F. Babu, V. Senthilkumar, J. S. Chung, W. M. Choi and Y. S. Kim, *RSC Adv.*, 2015, **5**, 29159–29166.
41 J. Y. Park, P. Daksha, G. H. Lee, S. Woo and Y. Chang, *Nanotechnology*, 2008, **19**, 365603.
42 R. Zirbs, A. Lassenberger, I. Vonderhaid, S. Kurzhals and E. Reimhult, *Nanoscale*, 2015, **7**, 11216–11225.
43 U. I. Tromsdorf, O. T. Bruns, S. C. Salmen, U. Beisiegel and H. Weller, *Nano Lett.*, 2009, **9**, 4434–4440.
44 H. Wei, N. Insin, J. Lee, H.-S. Han, J. M. Cordero, W. Liu and M. G. Bawendi, *Nano Lett.*, 2011, **12**, 22–25.
45 M. Lundqvist, J. Stigler, T. Cedervall, T. Berggård, M. B. Flanagan, I. Lynch, G. Elia and K. Dawson, *ACS Nano*, 2011, **5**, 7503–7509.
46 A. Salvati, A. S. Pitek, M. P. Monopoli, K. Prapainop, F. B. Bombelli, D. R. Hristov, P. M. Kelly, C. Aberg, E. Mahon and K. A. Dawson, *Nat. Nanotechnol.*, 2013, **8**, 137–143.
47 F. Alexis, E. Pridgen, L. K. Molnar and O. C. Farokhzad, *Mol. Pharmaceutics*, 2008, **5**, 505–515.
48 G. Yang, K. Kim, W. Wang, B. Chen, H. Mattoussi and D. T. Hallinan Jr, *Macromol. Chem. Phys.*, 2018, **219**, 1700417.
49 N. K. Kwon, H. Kim, T. J. Shin, K. Saalwächter, J. Park and S. Y. Kim, *Macromolecules*, 2020, **53**, 4836–4844.
50 S. Woo, S. Kim, H. Kim, Y. W. Cheon, S. Yoon, J.-H. Oh and J. Park, *Nanomaterials*, 2021, **11**, 3068.
51 Z. Zhou, C. Wu, H. Liu, X. Zhu, Z. Zhao, L. Wang, Y. Xu, H. Ai and J. Gao, *ACS Nano*, 2015, **9**, 3012–3022.
52 J. Park, J. Nam, N. Won, H. Jin, S. Jung, S. Jung, S.-H. Cho and S. Kim, *Adv. Funct. Mat.*, 2011, **21**, 1558–1566.
53 H. Soo Choi, W. Liu, P. Misra, E. Tanaka, J. P. Zimmer, B. Itty Ipe, M. G. Bawendi and J. V. Frangioni, *Nat. Biotechnol.*, 2007, **25**, 1165–1170.
54 B. Du, M. Yu and J. Zheng, *Nat. Rev. Mater.*, 2018, **3**, 358–374.